

# THE END OF THE DARK AGES IN MOND

S. Stachniewicz<sup>1</sup>, M. Kutschera<sup>1,2</sup>

<sup>1</sup>*Astrophysics Division, H.Niewodniczański Institute of Nuclear Physics, ul. Radzikowskiego 152, 31-342 Kraków, Poland*

<sup>2</sup>*Institute of Physics, Jagiellonian University, ul. Reymonta 4, 30-059 Kraków, Poland*

## ABSTRACT

We study the evolution of a spherically symmetric density perturbation in the Modified Newtonian Dynamics (MOND) model applied to the net acceleration over Hubble flow. The background cosmological model is a  $\Lambda$ -dominated, low- $\Omega_b$  Friedmann model with no Cold Dark Matter. We include thermal processes and non-equilibrium chemical evolution of the collapsing gas. We find that under these assumptions the first low-mass objects ( $M \leq 3 \times 10^4 M_\odot$ ) may collapse already for  $z \sim 30$ , which is in quite good agreement with the recent WMAP results. A lower value of  $a_0$  would lead to much slower collapse of such objects.

**Key words:** hydrodynamics – gravitation – instabilities – dark matter – early Universe.

## 1 INTRODUCTION

Recent developments in cosmological observations have led to the so-called cosmological concordance model with  $\Omega_b$  around 0.03,  $\Omega_m$  (dark+baryonic) around 0.3 and  $\Omega_\Lambda$  around 0.7. However, as the  $\Lambda$ CDM models are dominated by hypothetical vacuum energy and non-baryonic dark matter contributions, some scientists are looking for different solutions. Perhaps the most interesting alternative model is the Modified Newtonian Dynamics model (MOND) proposed by Milgrom (1983). It assumes that there is no non-baryonic dark matter (or it is negligible) and the apparent lack of matter is only due to the modification of dynamics or gravity for small accelerations ( $a \ll a_0$  where  $a_0$  is some constant). This model seems to work very well for spiral galaxies and many other types of objects (Sanders & McGaugh 2002). However, it carries with it some unresolved problems (e.g. lack of covariance).

The problem of the structure formation in MOND was also explored by Sanders (2001) and Nusser (2002), but they were interested in large cosmic structures and did not include gas effects. It is a good approximation for large scales, but gas effects play a crucial role in the small-scale structure formation.

Stachniewicz & Kutschera (2001b) studied possible implications of the MOND model for the formation of the very first objects in the Universe. However, there we had applied MOND to total gravitational acceleration, and this approach can lead to some paradoxes, e.g. time and the very occurrence of collapse hardly depend on the initial overdensity. In this paper, we attempt a different approach; namely, we apply MOND to the **net** acceleration over the Hubble flow only.

## 2 MOND VS STANDARD THEORY OF LINEAR PERTURBATIONS

If one wants to apply the MOND model to structure formation calculations, they encounter a number of difficulties. First of all, MOND is not a theory, but rather a phenomenological model. In its present form, MOND is inconsistent with General Relativity. Although Bekenstein (2004) found a relativistic gravitation theory that gives MOND-like predictions in the low-gravity limit, it needs to be verified.

MOND is a model that modifies either dynamics or gravity (in this paper we assume the latter). It introduces a new fundamental scale, usually called  $a_0$ . Gravitational fields much stronger than  $a_0$  are identical to their Newtonian limit  $g_N$ , and very weak fields are  $\sqrt{a_0 g_N}$ . According to Sanders & Verheijen (1998), the value of the fundamental acceleration scale is  $a_0 = 1.2 \times 10^{-8} \text{ cm/s}^2$ . More precisely, the strength of the gravitational field may be written as

$$\mu\left(\frac{g}{a_0}\right) \vec{g} = \vec{g}_N, \quad (1)$$

where  $\mu(x)$  is some function that interpolates between these two extreme cases. This function is not specified in the model. We have decided to apply the function used by Sanders & Verheijen (1998):

$$\mu(x) = \frac{x}{\sqrt{1+x^2}} \quad (2)$$

and, finally,

$$\vec{g} = \vec{g}_N \sqrt{\frac{1 + \sqrt{1 + \left(\frac{g}{a_0}\right)^2}}{2}} \quad (3)$$

where  $x = g_N/a_0$ .

The consequences of MOND for cosmology have not been studied in detail yet. Sanders (1998) suggested that because in the early Universe the MOND radius is much lower than that of the horizon, the evolution of the scale factor is described by the standard Friedmann equations. Also in the theory described by Bekenstein (2004) cosmological models are similar to the Friedmann ones so we follow this assumption and study the formation of the first objects in the Universe with modified dynamics.

We adopted this approach in Stachniewicz & Kutschera (2001b), but, as mentioned in the Introduction, this may lead to some paradoxes – in particular, even underdense regions of the Universe may collapse. In order to avoid that problem, we have tried another approach applying MOND to the **net** acceleration/deceleration over the Hubble flow. In this approach, only clouds with **positive** overdensity may stop their expansion and recollapse, so the final formula for gravitational acceleration (or deceleration) is

$$\mu\left(\frac{|\vec{g} - \vec{g}_H|}{a_0}\right) (\vec{g} - \vec{g}_H) = \vec{g}_N - \vec{g}_H, \quad (4)$$

where  $g_H$  is the deceleration (or acceleration) due to the Hubble flow.

## 2.1 Collapse of perfect gas

If we take perfect gas instead of the pressureless fluid, the evolution will look different because the effects of pressure will moderate the recollapse, especially for small systems. Since we assume spherical symmetry, Lagrangian coordinates are used.

In the Newtonian case, dynamics is governed by the following equations:

$$\frac{dM}{dr} = 4\pi r^2 \varrho, \quad (5)$$

$$\frac{dr}{dt} = v, \quad (6)$$

$$\frac{dv}{dt} = -4\pi r^2 \frac{dp}{dM} - \frac{GM(r)}{r^2}, \quad (7)$$

$$\frac{du}{dt} = \frac{p}{\varrho^2} \frac{d\varrho}{dt} + \frac{\Lambda}{\varrho}, \quad (8)$$

where  $r$  is the radius of a sphere of mass  $M$ ,  $u$  is the internal energy per unit mass,  $p$  is pressure and  $\varrho$  is mass density. Here, Eq.(5) is the continuity equation, (6) and (7) give acceleration and (8) accounts for energy conservation. The last term in Eq.(8) describes gas cooling/heating, with  $\Lambda$  being energy absorption (emission) rate per unit volume, given in detail in Stachniewicz & Kutschera (2001a).

We use the equation of state of perfect gas

$$p = (\gamma - 1)\varrho u, \quad (9)$$

where  $\gamma = 5/3$ , as the primordial baryonic matter after recombination is assumed to be composed mainly of monoatomic hydrogen and helium, with the fraction of molecular hydrogen  $H_2$  always less than  $10^{-3}$ .

In the case of modified gravity, equation (7) will look somewhat different:

$$\frac{dv}{dt} = -4\pi r^2 \frac{dp}{dM} - g_H - a_0 f\left(\frac{GM(r)}{a_0 r^2} - \frac{g_H}{a_0}\right), \quad (10)$$

where  $f(x)$  is inverse to function  $\mu(x)$  mentioned before, asymptotically equal to  $x$  for  $x \gg a_0$  and to  $\sqrt{a_0 x}$  for  $x \ll a_0$ , while  $g_H$  may be expressed as

$$g_H = \frac{1}{2} H_0^2 [(z+1)^3 \Omega_b + 2((z+1)^4 \Omega_r - \Omega_\Lambda)] r. \quad (11)$$

Here,  $H_0$  is the current value of the Hubble parameter,  $\Omega_b$ ,  $\Omega_r$  and  $\Omega_\Lambda$  are the current fractions of baryons, radiation and dark energy in terms of the critical density of the Universe, and  $z$  is the redshift.

## 2.2 Chemical reactions and thermal effects

In our calculations, we include all of the relevant thermal and chemical processes in the primordial gas. In this paper, we have taken into account nine species: H, H<sup>-</sup>, H<sup>+</sup>, He, He<sup>+</sup>, He<sup>++</sup>, H<sub>2</sub>, H<sub>2</sub><sup>+</sup> and e<sup>-</sup>. The abundance of various species changes with time due to chemical reactions, ionization and dissociation photoprocesses. The chemical reactions include such processes as ionization of hydrogen and helium by electrons, recombination of ions with electrons, formation of negative hydrogen ions, formation of H<sub>2</sub> molecules, etc. A full list of the relevant chemical reactions and appropriate formulae is given in Stachniewicz & Kutschera (2001a).

The time evolution of the number density of component  $n_i$  is described by the kinetic equation:

$$\frac{dn_i}{dt} = \sum_{l=1}^9 \sum_{m=1}^9 a_{lm} k_{lm} n_l n_m + \sum_{j=1}^9 b_{ji} \kappa_j n_j. \quad (12)$$

The first component on the right-hand side of this equation describes the chemical reactions, and the other one accounts for photoionization and photodissociation processes. Coefficients  $k_{lm}$  are reaction rates, quantities  $\kappa_n$  are photoionization or photodissociation rates, and  $a_{lm}$  and  $b_{ji}$  are numbers equal to 0,  $\pm 1$  or  $\pm 2$  depending on the reaction. All reaction rates, as well as photoionization and photodissociation rates are given in Stachniewicz & Kutschera (2001a).

The cooling (heating) function  $\Lambda_{cool}$  includes effects of collisional ionization of H, He and He<sup>+</sup>, recombination to H, He and He<sup>+</sup>, collisional excitation of H and He<sup>+</sup>, Bremsstrahlung, Compton cooling and cooling by de-excitation of H<sub>2</sub> molecules. The formulae for the heating/cooling contributions of various processes are given in Stachniewicz & Kutschera (2001a).

## 3 CODE USED IN THE SIMULATIONS AND INITIAL CONDITIONS

In the simulations we used the code described in Stachniewicz & Kutschera (2001a), based on those presented by Thoul & Weinberg (1995) and Haiman et al. (1996). This is a standard, one-dimensional, second-order accurate, Lagrangian finite-difference scheme. The only changes consist in the modification of gravity, with the dark matter fraction  $\Omega_{dm}$  set to zero. However, it was necessary to make significant changes in the initial conditions.

First of all, we started our calculations at the end of the radiation-dominated era. For  $\Omega_b = \Omega_m = 0.02/h^2$ ,  $z_{eq} = 485$  as given by the formula provided by Hu & Eisenstein (1998),  $z_{eq} = 2.50 \times 10^4 \Omega_0 h^2 \Theta_{2.7}^{-4}$ , where  $\Theta_{2.7} = T_\gamma/2.7K$ , assuming  $h = 0.72$  and  $T_\gamma = 2.7277$  K. We assumed that, like

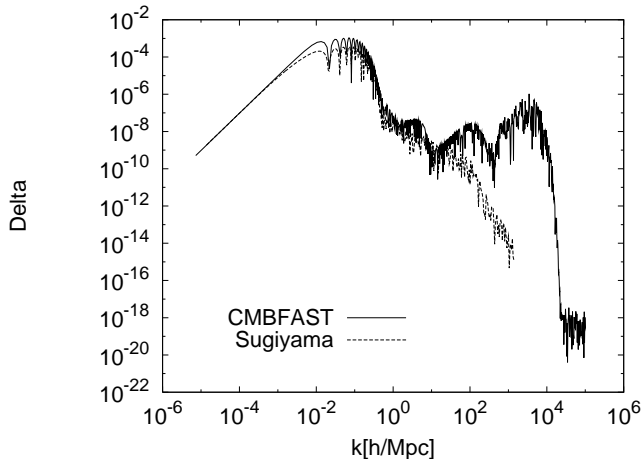


Figure 1. Matter power spectrum.

in the standard cosmology, initial overdensities may grow only in the matter-dominated era. We used our own code to calculate the initial chemical composition and initial gas temperature. When compared with the results obtained by Galli & Palla (1998), ours are very similar – the agreement is at the level of 10-20%. The difference is probably due to the fact that Galli and Palla had included more species (e.g. deuterium and lithium), and some reaction rates they used had been somewhat different.

It is necessary to specify the initial baryonic matter perturbations,  $\delta$ . We have decided to take values of the order of the contribution to the baryonic matter power spectrum at a given scale and redshift. The problem is that at these scales the power spectrum is known very roughly, as there are no observational data and the relevant physical processes are not known very well. The power spectrum may be calculated using the CMBFAST program by Seljak & Zaldarriaga (1996)  $\Delta(k) = \sqrt{4\pi d_{norm}^2 k^4 t_f(k, z)^2}$ , where  $t_f$  is the transfer function,  $k$  is the wavenumber and the value of normalization constant  $d_{norm}^2$  is obtained from CMBFAST. We also included the output of the CMB anisotropy program written by N. Sugiyama, received from the author. The results are shown in Fig. 1.

The most interesting for us are the comoving scales around 10 kpc. For these scales, both outputs differ significantly by a factor of 100. We decided to take our initial overdensity from in between, i.e. equal to  $10^{-9}$ . As we will show, these differences do not affect our results significantly.

We apply the initial density profiles in the form of a single spherical Fourier mode, also used by Haiman et al. (1996)

$$\varrho_b(r) = \Omega_b \varrho_c \left(1 + \delta \frac{\sin kr}{kr}\right), \quad (13)$$

where  $\varrho_c$  is the critical density of the Universe,  $\varrho_c = 3H^2/8\pi G$ , with  $H$  being the actual value of the Hubble parameter.

For this profile, there exist two distinguished radius values, namely  $R_0$  and  $R_z$ , which correspond to the first zero and the first minimum of the function  $\sin(kr)/kr$ , respectively. Inside the sphere of radius  $R_0 = \pi/k$  which contains mass  $M_0$ , the local density contrast is positive. The mass  $M_0$  and the radius  $R_0$  will be referred to as the cloud mass and

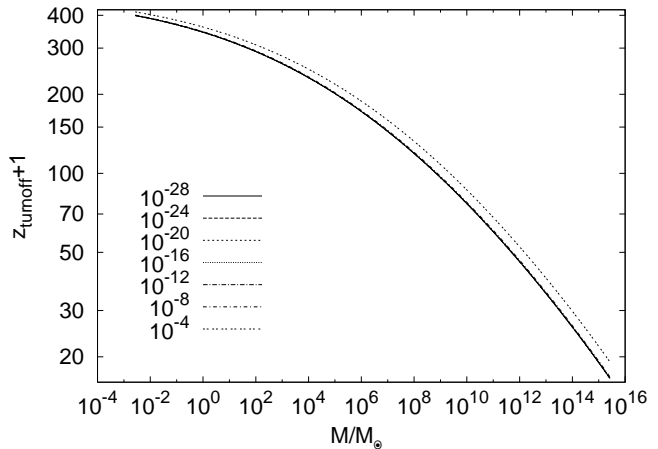


Figure 2. Turnaround times for shells of various masses and initial overdensities

the cloud radius, respectively. The local density contrast is negative for  $R_z > r > R_0$ , with average density contrast vanishing for the sphere of radius  $R_z = 4.49341/k$  and mass  $M_z$ . According to the gravitational instability theory in the expanding Universe, the shell of radius  $R_z$  will expand together with the Hubble flow, not undergoing any additional deceleration. This is why we regard this profile as very convenient in numerical simulations. Namely, it eliminates the numerical edge effects and the mentioned shell simply follows the Hubble expansion of the Universe. Thus, it can be regarded as the perturbation boundary, with mass  $M_z$  referred to as the bound mass.

It is worth noting that for radii not greater than  $3/4R_0$  this profile is very similar to the Gaussian profile

$$\varrho_i(r) = \Omega_i \varrho_c \left[1 + \delta_i \exp\left(\frac{-r^2}{2R_f^2}\right)\right] \quad (14)$$

with  $R_f = 1/2R_0$ .

As the initial velocity, we use the Hubble velocity:

$$v(r) = Hr. \quad (15)$$

#### 4 PRESSURELESS COLLAPSE IN MOND

We decided to describe the case of a pressureless collapse in MOND as this makes it easier to understand why the results shown in the next section hardly depend on the initial overdensities. It is much easier to trace shells since each shell may be treated separately, so it is enough to trace the evolution of a single shell with some initial overdensity and constant mass inside. Equation 10 is reduced to

$$\frac{dv}{dt} = -g_H - a_0 f\left(\frac{GM(r)}{a_0 r^2} - \frac{g_H}{a_0}\right), \quad (16)$$

where the expression for  $g_H$  was shown in Eq. 11. We wrote a small program calculating the turnaround times for shells of various masses and initial overdensities. It starts at the beginning of the matter-dominated era with the initial velocity being the Hubble velocity ( $v = Hr$ ). The results are shown in Fig. 2.

As we can see, for initial overdensities of  $10^{-8}$  and lower, the results are almost indistinguishable and not very different from those for  $10^{-4}$ . This looks very odd, but it reflects the fact that a smaller overdensity means that the shell is very deep in the MOND regime and its behaviour is strongly nonlinear. Now let us assume that a shell is always in the MOND regime. For pure MOND Eq. 16 takes the form

$$\frac{dv}{dt} = -g_H - \sqrt{a_0 \left( \frac{GM(r)}{r^2} - g_H \right)}. \quad (17)$$

It is a nonlinear equation, especially in the low overdensity limit. This becomes obvious if we change variables. Instead of  $r$ , let us put  $(R - r)$ , where  $R$  is the radius corresponding to the mass  $M$  in a homogenous Universe. In other words,  $r$  is related to the actual overdensity  $\delta$  and if it is much lower than  $R$ , it may be expressed as  $\delta = 3r/R$ . Given that, equation 17 may be written as

$$\frac{d^2r}{dt^2} = \sqrt{3a_0 G \frac{M}{R^2} \frac{r}{R}}. \quad (18)$$

Now we may express mass in terms of the cosmological parameters, redshift and  $R$ , and we get

$$\frac{d^2r}{dt^2} = \sqrt{\frac{3}{2} \Omega_b a_0 H_0^2 (z+1)^3 r}. \quad (19)$$

Redshift  $z$  is a function of time, and if we put  $d\tau = [\frac{3}{2} \Omega_b a_0 H_0^2 (z+1)^3]^{1/4} dt$ , we finally obtain

$$\frac{d^2r}{d\tau^2} = \sqrt{r}. \quad (20)$$

## 5 RESULTS

We performed seventeen runs. The first eight were for the ‘standard’ value of  $a_0$  ( $1.2 \times 10^{-8} \text{ cm/s}^2$ ), various masses of the cloud ( $10^3 M_\odot$ ,  $3 \times 10^3 M_\odot$ ,  $10^4 M_\odot$  and  $3 \times 10^4 M_\odot$ ) and initial overdensities ( $10^{-9}$  and  $10^{-8}$ , the next three were for some lower value of  $a_0$  ( $1.2 \times 10^{-9} \text{ cm/s}^2$ ), initial overdensity  $10^{-9}$  and masses of the cloud equal to  $3 \times 10^3 M_\odot$ ,  $10^4 M_\odot$  and  $3 \times 10^4 M_\odot$ , while the last one was for the ‘standard’ value of  $a_0$  but with no  $\text{H}_2$  cooling. The results are shown in Figs. 3-11.

Most of these figures show trajectories of shells enclosing 7%, 17%, 27% ... 97% of the total mass: Figs. 3-6 for the ‘standard’  $a_0$  and  $10^{-9}$  overdensity and Figs. 9-11 for the ‘low’  $a_0$ ,  $10^{-9}$  overdensity, respectively. In addition, Fig. 7 shows temperatures of the same shells as in Fig. 3 and Fig. 8 shows the chemical evolution for shells enclosing  $0.12 M_z$ , both figures showing runs for the ‘standard’  $a_0$ ,  $10^{-9}$  overdensity and  $M = 10^3 M_\odot$  (the results for the other masses are very similar). The results for  $10^{-8}$  are almost indistinguishable and the run with greater mass ( $M = 10^5 M_\odot$ ) but no  $\text{H}_2$  cooling showed no collapse.

The results show that:

- as expected, the difference in behaviour between clouds with  $10^{-9}$  and  $10^{-8}$  overdensities is very tiny, thus the results are much less sensitive to the initial density contrast than in CDM
- more massive clouds collapse faster
- speed of collapse depends very strongly on  $a_0$

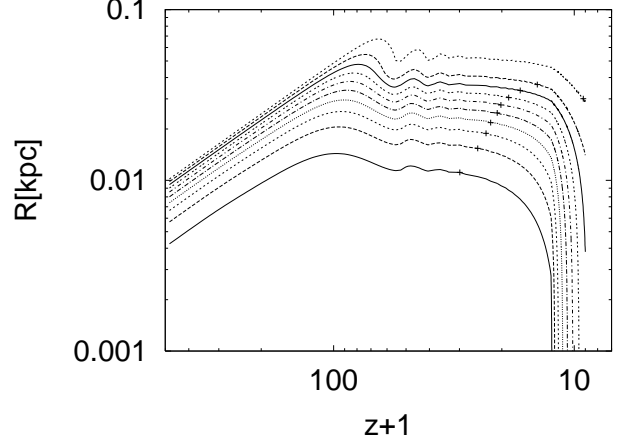


**Figure 3.** Shell trajectories for the ‘standard’  $a_0$ ,  $10^{-9}$  overdensity,  $M = 10^3 M_\odot$ .

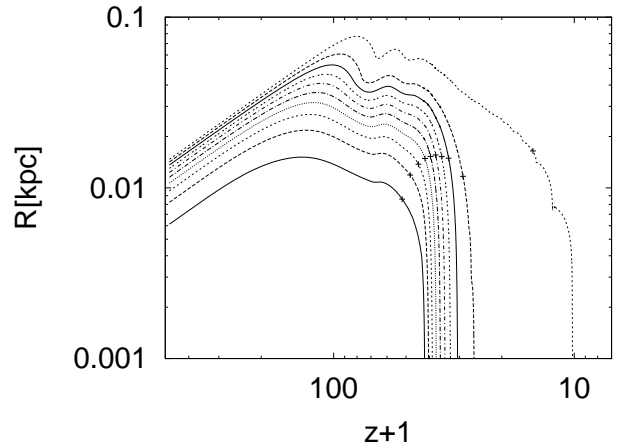


**Figure 4.** Shell trajectories for the ‘standard’  $a_0$ ,  $10^{-9}$  overdensity,  $M = 3 \times 10^3 M_\odot$ .

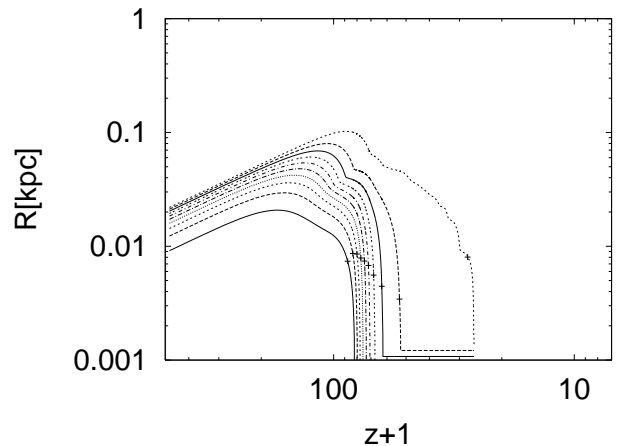


**Figure 5.** Shell trajectories for the ‘standard’  $a_0$ ,  $10^{-9}$  overdensity,  $M = 10^4 M_\odot$ .

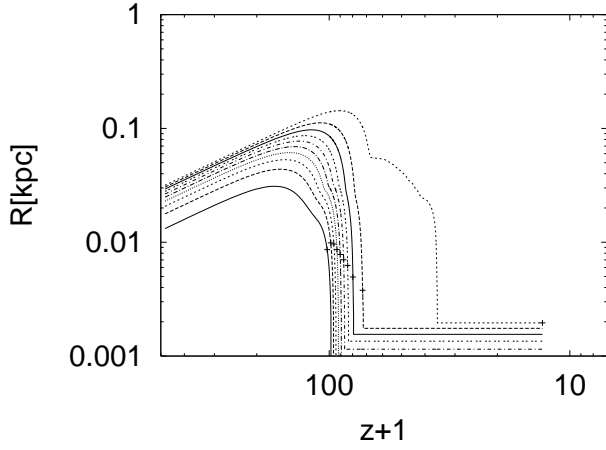


**Figure 6.** Shell trajectories for the ‘standard’  $a_0$ ,  $10^{-9}$  overdensity,  $M = 3 \times 10^4 M_\odot$ .

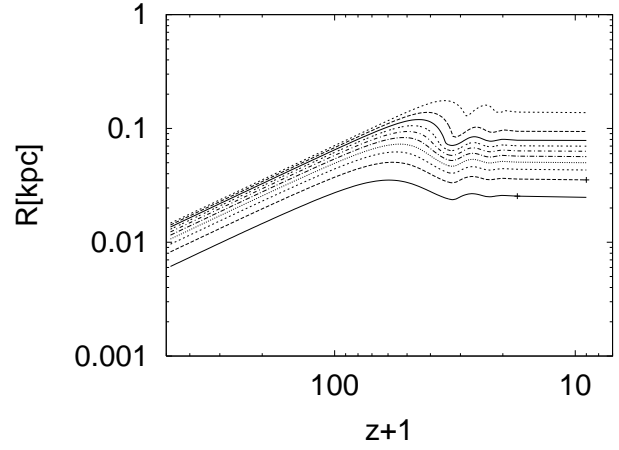


**Figure 9.** Shell trajectories for the ‘low’  $a_0$ ,  $10^{-9}$  overdensity,  $M = 3 \times 10^3 M_\odot$ .

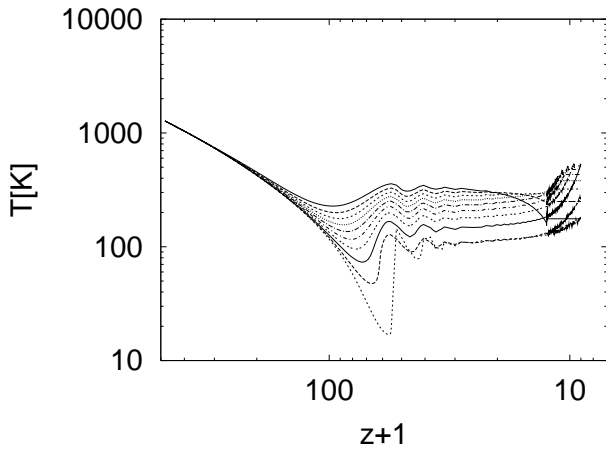


**Figure 7.** Shell temperatures for the ‘standard’  $a_0$ ,  $10^{-9}$  overdensity,  $M = 10^3 M_\odot$ .

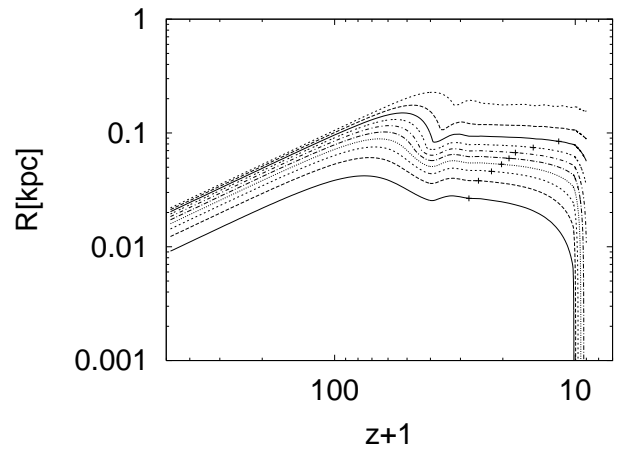


**Figure 10.** Shell trajectories for the ‘low’  $a_0$ ,  $10^{-9}$  overdensity,  $M = 10^4 M_\odot$ .

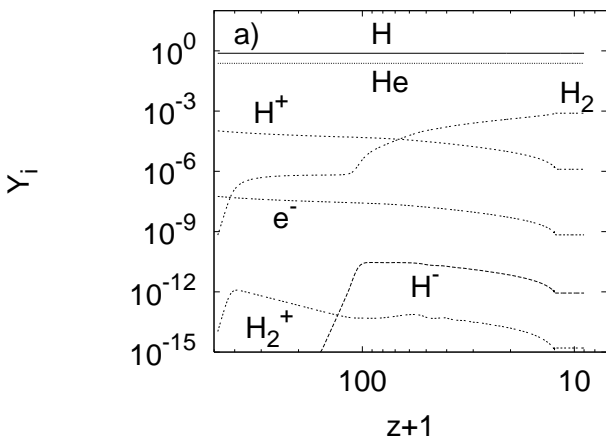


**Figure 8.** Chemical evolution for the ‘standard’  $a_0$ ,  $10^{-9}$  overdensity,  $M = 10^3 M_\odot$ .

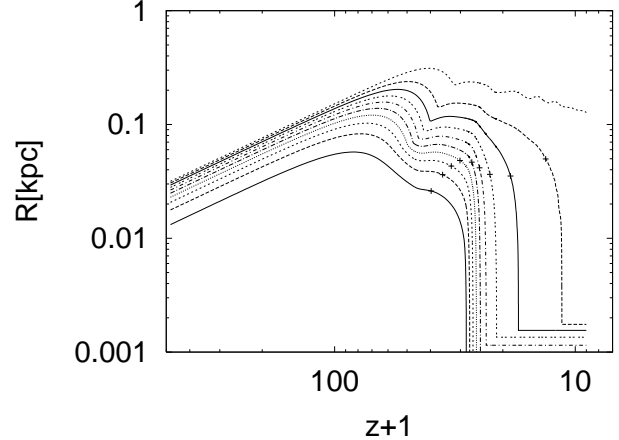


**Figure 11.** Shell trajectories for the ‘low’  $a_0$ ,  $10^{-9}$  overdensity,  $M = 3 \times 10^4 M_\odot$ .

- like in the CDM models, H<sub>2</sub> cooling is necessary to collapse
- like in the CDM models, due to the adiabatic cooling/heating, the shell temperature behaviour is opposite to that of the shell radii; then H<sub>2</sub> cooling becomes important and the shells collapse; a higher mass of the cloud means higher virial temperature and faster collapse
- chemical evolution is quite typical but because the collapse is very violent, it speeds up chemical reactions; however, the final abundances of various species are not very different from the predictions of the other models, e.g. the final abundance of H<sub>2</sub> is of the order of 10<sup>-3</sup>.

It may appear that during the collapse, shell temperatures do not fall as deep as in CDM models, but this is a numerical artefact only. The reason is, as in Thoul & Weinberg (1995), that in our code – if a shell falls below some ‘small’ radius  $r_c$  – we treat it as ‘collapsed’: we artificially stop its dynamical and chemical evolution, assigning some small radius, freezing the temperature and including its gravitational field only. A collapse in MOND is very violent, so gas shells have not enough time to cool down until their temperature is frozen by the code.

We performed many other runs as well, e.g. with initial overdensities greater than 10<sup>-4</sup>, but the results were very similar. The reason for this is that, as shown in the previous section, in the absence of gas pressure, any positive initial overdensity lower than some reasonable value leads to a very similar turnaround time. Because at this stage of evolution the gas effects are not yet very important, this also applies to the evolution with all physical processes included. This means that in the approximation the turnaround time depends on mass. Then the cloud starts its initial collapse, but it gets virialised and the time between the virialisation and the final collapse depends on mass again, i.e. the bigger the mass, the faster the collapse.

The Wilkinson MAP results suggest that reionization occurred at around  $z \sim 20$ . This means that the first bound objects must have been formed even earlier, perhaps at around  $z \sim 30$ . Our recent simulations (Stachniewicz & Kutschera 2003) show that if we assume the  $\Lambda$ CDM models and take the recent estimates of  $\Omega_M$  and  $\Omega_\Lambda$ , a direct formation of low-mass objects that could possibly reionize the Universe before  $z \sim 10$  is very unlikely. Moreover, we doubt whether the inclusion of possible fragmentation of greater clouds could speed up the collapse enough – even if some low-mass cloud has greater overdensity than the directly forming ones, it still needs some time to cool down.

In contrast, MOND seems to provide a good way to solve that problem. For the ‘standard’ value of  $a_0$  clouds of mass  $3 \times 10^3 M_\odot$  or heavier may collapse at around  $z \sim 30$ , so that they or their cores may have formed the first stars and quasars. For lower  $a_0$ , only objects of mass  $3 \times 10^4 M_\odot$  or greater may be formed directly before  $z \sim 30$ . We think this favours the ‘standard’ value but one would need to perform full 3-D simulations to give a more definite answer.

It may be surprising that in our simulations more massive objects form earlier, but it is due to the gas pressure, which is more important for less massive objects. If we skip that term in Eq. 7, less massive objects stop their expansion and recollapse faster than the more massive ones. However,

this is not the case for the Large Scale Structure: on these scales, gas effects may be neglected, and although in general the MOND effects are smaller, the rms fluctuations decrease so that such objects stop their expansion more slowly.

## 6 CONCLUSIONS

If our assumptions about MOND are correct, its predictions seem to be more consistent with the the early reionization suggested by the WMAP results (Bennett et al. 2003; Spergel et al. 2003) than the ones of the most recent  $\Lambda$ CDM models. This does not prove that MOND is correct and  $\Lambda$ CDM is not. However, this suggests that cosmologists should perhaps pay more attention to MOND, because it seems to be an interesting alternative to models with non-baryonic dark matter.

## ACKNOWLEDGMENTS

We are very grateful to Uroš Seljak for answering our questions about CMBFAST, to N. Sugiyama for sending us the output of his CMB anisotropy program, and to R.H. Sanders for his comments about the role of the Silk damping.

Our work was partially supported by the Polish State Committee for Scientific research under grants nrs. 2P03B 11024 and PBZ-KBN-054/P03/02.

## REFERENCES

- Bekenstein J. D., 2004, *Phys. Rev. D*, 70, 3509  
 Bennett C. L. et al., 2003, *ApJS*, 148, 1B  
 Eisenstein D. J., Loeb A., 1995, *ApJ*, 443, 11  
 Galli D., Palla F., 1998, *A&A*, 335, 403  
 Haiman Z., Thoul A. A., Loeb A., 1996, *ApJ*, 464, 523  
 Hu W., Eisenstein D. J., 1998, *ApJ*, 498, 497  
 Kolb E. W., Turner M. S., 1990, *The Early Universe*, Addison-Wesley  
 Milgrom M., 1983, *ApJ*, 270, 371  
 Nusser A., 2002, *MNRAS*, 331, 909  
 Sanders R. H., 1998, *MNRAS*, 296, 1009  
 Sanders R. H., 2001, *ApJ*, 560, 1  
 Sanders R. H., McGaugh S. S., 2002, *ARA&A*, 40, 263  
 Sanders R. H., Verheijen M. A. W., 1998, *ApJ*, 503, 97  
 Seljak U., Zaldarriaga M., 1996, *ApJ* 469, 437  
 Spergel D. N. et al., 2003, *ApJS*, 148, 175S  
 Stachniewicz S., Kutschera M., 2001, *Acta Phys. Pol. B* 32, 227  
 Stachniewicz S., Kutschera M., 2001, *Acta Phys. Pol. B*, 32, 3629  
 Stachniewicz S., Kutschera M., 2003, *MNRAS*, 339, 616  
 Thoul A. A., Weinberg D. H., 1995, *ApJ*, 442, 480